Electronic Excited States and UV–Vis Absorption Spectra of the Dihydropyrene/Cyclophanediene Photochromic Couple: a Theoretical Investigation

Rudraditya Sarkar, Marie-Catherine Heitz, Guy Royal, Martial Boggio-Pasqua

Electronic Excited States and UV-Vis Absorption Spectra of the Dihydropyrene/Cyclophanediene Photochromic Couple: A Theoretical Investigation

*Rudraditya Sarkar,[A] Marie-Catherine Heitz,[A] Guy Royal,[B] Martial Boggio-Pasqua[A,]**

[A] Laboratoire de Chimie et Physique Quantiques, UMR 5626, IRSAMC, CNRS et Université Toulouse 3, 118 route de Narbonne, 31062 Toulouse, France

[B] Université Grenoble Alpes, CNRS, DCM, F-38000 Grenoble, France

martial.boggio@irsamc.ups-tlse.fr

Abstract. The dihydropyrene (DHP) / cyclophanediene (CPD) is a fascinating photoswitchable organic system displaying negative photochromism. Upon irradiation in the visible region, the colored DHP can be converted to its open-ring CPD colorless isomer, which can be converted back to DHP by UV light. DHP and CPD thus possess very different absorption spectra whose absorption bands have never been assigned in detail so far. In this work, we characterize the vertical electronic transitions of the first six and seven excited states of DHP and CPD, respectively, aiming for a realistic comparison with experiment. We used state-of-the-art electronic structure methods (e.g., CASPT2, NEVPT2, XMCQDPT2, ADC(3)) capable of describing differential electron correlation. Vertical transition energies were also computed with time-dependent density functional theory (TD-DFT) and compared to these accurate methods. After the reliability of TD-DFT was validated for the main optical transitions, this efficient method was used to simulate the absorption spectra of DHP and CPD in the framework of the Franck-Condon Herzberg-Teller (FCHT) approximation and also using the nuclear ensemble (NE) approach. Overall, for both methods,

the simulated absorption spectra reproduce nicely the main spectral features of the DHP and CPD isomers, that is, the main four absorption bands of increasing intensity of DHP and the absorption rise below 300 nm for CPD.

1. INTRODUCTION

Dihydropyrenes (DHPs) are remarkable photochromic compounds.[1] The core of these systems is made of a quasi-planar 14 π conjugated annulene. Upon irradiation in the visible range, DHPs are changed into their cyclophanediene (CPD) open-ring isomers, which in turn can be converted back to the DHP closed-ring forms upon UV irradiation or thermally (Scheme 1), making this photoswitch a remarkable example of negative photochromism (i.e., the thermodynamically stable form corresponds to the colored state).[2] The introduction of redox-active units can also allow for electrochemical control of the switching process.[3] DHPs with electron-withdrawing groups may also play the role of oxygen photosensitizer.[4,5] As a consequence of their original behavior, DHPs have been exploited to develop multiphotochromic architectures for multistate switches,[6,7] mixed valence-state compounds for photoswitchable electronic communication devices,[8,9] hybrid compounds for multifunctional materials,[10,1112,13] photo-switchable single-molecule junctions,[14,15,16,17] devices for logic gates[18] and derivatives operating in the near infra-red (NIR) region for biological applications.[19]

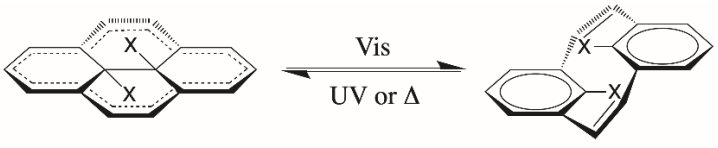

Scheme 1. The dihydropyrene (DHP) / cyclophanediene (CPD) photochromic couples considered in this study.

Over the past decades, a large number of DHP/CPD derivatives have been designed and synthesized in order to improve their thermal stability and their photoswitching efficiency,[20,21,22,23,24,25,26,27] while trying

to understand the photoisomerization mechanism.[28,29,30,31,32] The implication of a biradicaloid intermediate has been evidenced[29,33] and confirmed theoretically.[31] Unlike many other photochromic compounds for which the photoswitching mechanism can be described by a two-state problem,[34,35,36,37,38,39] DHPs clearly involve several electronic excited states of different character in the DHP to CPD photoconversion.[31] While the precise role of these states in the DHP photodynamics still needs to be uncovered, a first challenging step from a theoretical perspective is the accurate description of their associated electronic structures and relative energies. Surprisingly, there are very few studies devoted to the description of these electronic excited states and their implications on the UV-vis absorption spectra of the DHP and CPD isomers.[31,40] This is most probably due to the notorious difficulty to have a balanced description of the electron correlation in excited states of different character.[41,42,43,44] The challenge here is to use advanced electronic structure methods capable of describing the electron correlation with the same relative accuracy in order to obtain reliable excitation energies and ordering of states of different nature. In this context, the use of the complete active space self-consistent field (CASSCF) combined with a second-order perturbation theory (CASPT2) treatment using the CASSCF wavefunction as a reference has become the most popular and successful method for efficient and accurate calculations of excited states of small to medium-sized molecules.[45,46,47] However, the success of this approach depends on the choice of the set of active orbitals.[48] For larger systems, single reference time-dependent density functional theory (TD-DFT) is widely applied but its accuracy depends on the chosen functional and nature of the excited states.[49]

The DHP/CPD photochromic couple represents a fascinating molecular system to compare state-of-the-art methods in a difficult test case. We chose the simplest possible DHPs to carry out this work, that is dihydropyrene **1c** and dimethyldihydropyrene **2c** and their corresponding CPD isomers **1o** and **2o** (Scheme 1). Although DHP **1c** can easily lose its internal hydrogen atoms to form pyrene,[50] **1c**/**1o** would constitute a good model system for studying the photoisomerization of DHP into CPD if this model system presents the same excited-state features as the target system **2c**/**2o**. In this study, we aim at describing and assigning the first absorption bands of the DHP/CPD couple. This implies to describe reliably all the

electronic states participating in these absorption features. To achieve this task, we thus compare different levels of theory ranging from accurate multiconfigurational wavefunction-based methods to DFT-based calculations in order to describe the vertical transition energies of **1c** and **2c** and of their corresponding open-ring CPDs **1o** and **2o**. Then, we simulate the absorption spectra of the DHP and CPD isomers using either a vibrationally-resolved or a nuclear ensemble (NE) approach and compare them with the experimental ones.

2. COMPUTATIONAL DETAILS

Vertical transition energies of DHPs **1c** and **2c** and of CPDs **1o** and **2o** were computed at various levels of theory. Multireference perturbation theories such as the second-order complete active space perturbation theory (CASPT2),[51] its multi-state variant (MS-CASPT2),[52] the *n*-electron valence state perturbation theory (NEVPT2),[53] its quasi-degenerate extension (QD-NEVPT2)[54] and the extended multiconfigurational quasi-degenerate perturbation theory (XMCQDPT2)[55] were used based on a reference CASSCF wavefunction with all valence π orbitals included in the active space. For **1c** and **2c**, the active space thus comprises (14e,14o), whereas for **1o** and **2o** it is composed of (16e,16o). State-averaged CASSCF wavefunctions were used, averaging over the lowest two ^1A_g states, two ^1A_u states, four ^1B_u states and two ^1B_g states. All CASPT2 calculations were carried out within the MOLCAS 8.0 package[56] using a standard IPEA shift[57,58] of 0.25 a.u. and an imaginary level shift[59] of 0.1 a.u. to avoid intruder states. The Cholesky decomposition[60] with a threshold of 10^{-6} a.u. was used to speed up the evaluation of the two-electron integrals. All NEVPT2 calculations were performed in the strongly contracted version of the method using the chain-of-spheres approximation[61] as implemented in ORCA 4.0.1.[62] The NEVPT2 calculations could not be run with a (16e,16o) active space for such system sizes and thus were only performed for DHPs which only require (14e,14o). Due to intrinsic limitations of the implementation in FIREFLY 8.2.0,[63] XMCQDPT2 could not be performed over the four coupled ^1B_u states with a (16e,16o) active space. So for the transitions to these states in **1o** and **2o**, the optimized SA4-CASSCF(16,16) orbitals (corresponding to the complete valence π active space, which provides better

orbitals than the ones obtained at SA4-CASSCF(14,14) level) were used but only a CASCI(14e,14o) wavefunction served as a reference. In addition, for (16e,16o) active space, XMCQDPT2 had to be performed with a selection of the most prominent 8 10^6 configurations in the configuration interaction expansion. All these multireference perturbation theory calculations were performed using the cc-pVTZ basis set[64] on CASSCF/cc-pVTZ ground-state geometries (Tables S1-S4) optimized with MOLPRO[65].

Single-reference second- and third-order algebraic diagrammatic construction (ADC) approaches[66,67] have been applied on the studied systems in conjunction with the cc-pVDZ basis set.[64] Note that we could not run these calculations with the cc-pVTZ basis set nor could we perform the more accurate third-order response coupled-cluster (CC3)[68,69,70,71] method. The resolution-of-the-identity approximation was used as implemented in QCHEM 4.4.[72] TD-DFT calculations were performed using various hybrid and long-range corrected functionals using the GAUSSIAN 09 program package.[73] These include B3LYP,[74] B3PW91,[74,75] PBE0,[76] TPSSh,[77] M06,[78] M06-2X,[78] CAM-B3LYP[79] and ωB97XD.[80] The 6-311G(d,p) basis set was used and vertical transition energies were computed within the random phase approximation at the B3LYP ground-state optimized geometries.

The vibrationally-resolved absorption spectra of the first four excited states of DHPs **1c** and **2c** and of four excited states of **1o** were calculated following the formalism of Barone and co-workers[81] as implemented in GAUSSIAN 09.[73] These spectra are computed within the Franck-Condon Herzberg-Teller (FCHT) formalism taking into account a linear dependence of the transition dipole moment on the nuclear coordinates. The main issue to calculate the FC integrals lies in the fact that each vibrational wavefunction (ground and excited state) is expressed within a different set of normal coordinates. This is overcome following a linear transformation procedure to represent one set of coordinates (e.g., ground state) with respect to the other set (e.g., excited state) as proposed by Duschinsky.[82] This transformation is treated as a good approximation only when the considered molecule undergoes minute changes during the electronic transition. Analysis of the spectrum provides information on the assignment of the vibrational modes responsible for the vibronic transitions.

The present algorithm requires as an input the normal modes at the initial ground-state minimum (S_0) and the normal modes at the final excited state minimum (S_n). The ground state minima and normal modes were obtained at the B3LYP/6-311G(d,p) level of theory. The excited state geometries (S_1, S_2, S_3 and S_4) of **1c** and **2c** were optimized with TD-CAM-B3LYP using the same basis set. Numerical frequency calculations were then performed to obtain the normal modes of the excited states. The main geometrical parameters of the ground and first four excited states of **1c** and **2c** are given in Tables S5 and S6, respectively. The ground and excited structures of **1c** and **2c** all belong to the C_{2h} symmetry point group. This is also the case for **1o** (Table S7) but not for **2o** for which some excited states do not preserve the C_{2h} symmetry. Thus, the calculations of vibronically-resolved absorption spectra of **2o** could not be performed. However, the very similar absorption spectra of **1c** and **2c** and also the comparable vertical transition energies between **1o** and **2o** suggest that the overall absorption band structures of **1c** and **1o** and their dimethyl-substituted analogues should be very similar. All the FCHT absorption spectra are simulated at 0 K using a spectral resolution of 8 cm^{-1} and a half-width at half-maximum of 135 cm^{-1} (with a Gaussian convolution function).

In addition to the calculations of the FCHT absorption spectra, we have also performed the simulations of the absorption spectra of **2c** and **2o** following the excitations of an ensemble of nuclear (NE) geometries at their respective ground state nuclear distributions. The main advantage of NE method[83] resides in its in-built post-Condon approximation by evaluating transition moments at geometries distorted from the equilibrium position. Thus, improvement of the spectral properties is expected, such as vibrational broadening, effects of dark electronic states (e.g., role of the ^1B_g states in the photoabsorption spectra of CPDs) and absolute spectral intensities. The ground-state phase-space of **2c** and **2o** were sampled by following quantum sampling[84] using a harmonic-oscillator Wigner distribution at 0 K and selecting respectively 1000 and 900 nuclear geometries and momenta to compute the absorption spectra. The convergence of the spectra was carefully checked against the number of sampled nuclear geometries. As for the calculations of the FCHT absorption spectra, the normal modes of the ground state minimum structures of **2c** and **2o** were taken from the B3LYP/6-311G(d,p) level of theory and vertical transition

energies and oscillator strengths for ten excited states at each ensemble geometry were computed using TD-CAM-B3LYP/6-311G(d,p). The photoabsorption cross sections were then generated from these data using a normalized Lorentzian line shape and a phenomenological spectral broadening of 0.1 eV with a spectral line resolution of 5 10^{-5} eV (0.4 cm^{-1}). The error in the absorption cross section due to the statistical sampling was also evaluated and plotted along with the absorption cross section. The photoabsorption cross sections were computed using NEWTON-X[85,86,87] interfaced with GAUSSIAN 09[73] for the evaluation of the vertical transition energies and oscillator strengths with TD-DFT.

3. RESULTS AND DISCUSSIONS

The UV-Vis absorption spectra of simple DHPs like **2c** show four absorption bands of increasing intensity, while those of the corresponding CPDs are not as well structured.[29] For illustration, a typical example is shown in Figure 1 for a bis(t-butyl) DHP and its corresponding CPD in cyclohexane. The effect of the t-butyl substituents and of the solvent are fairly small (see Table S8 for the effect of t-butyl substituents and cyclohexane solvent on vertical transition energies). The lowest energy band of DHPs is observed around 640 nm and corresponds to the band with the lowest absorbance. A second more intense band is observed in the blue region of the visible spectrum around 470-480 nm. Two higher energy peaks are located in the UV region around 380 and 340 nm. In CPDs, no absorption can be detected in the visible range and the absorption spectra are shifted to the UV region (the main absorption bands are found below 300 nm) because of the decreased aromaticity following the loss of the annulene ring and due to the steplike nature of the cyclophane, which prevents extended conjugation.

In the following, we first present the results of vertical transition energy calculations using different levels of theory and compare these energies with the position of the absorption maxima observed experimentally. We then simulate the absorption spectra in order to describe their associated band shape.

Vertical transition energies. The calculations of vertical transition energies for DHPs **1c** and **2c** and for CPDs **1o** and **2o** using various levels of theory are collected in Tables 1 to 6, respectively. All these excitation energies correspond to valence $\pi \rightarrow \pi^*$ transitions.

Closed-ring isomer. Let us first consider the case of the DHP closed-ring isomer. In the following, the XMCQDPT2 values are given unless otherwise stated, as this level of theory gives the best overall agreement with the experimental values (vide infra). A direct comparison of the nature of the electronic states and of the vertical transition energies between **1c** and **2c** (Tables 1 and 2) show that these two DHPs share the same set of electronic states in the same energetic order. The main difference is that vertical transition energies are slightly blue shifted in **1c** compared to **2c** (by ca. 0.05 eV on average). The first singlet excited state S_1 is the A_u^+ state (denoted $S_1(1^1A_u)$ hereafter) described as a plus (in-phase) combination of the HOMO–1→LUMO and HOMO→LUMO+1 excitations. It corresponds to the ^1L_b covalent state according to Platt's nomenclature.[88] This state is located at 1.978 and 1.954 eV above S_0 for **1c** and **2c**, respectively. This is in very good agreement with the maximum of the first absorption band observed in **2c** at 641 nm (1.934 eV).[29] Note that this state does not lead to photoisomerization and is responsible for DHP fluorescence.[31]

The second singlet excited state is the B_u^- state (denoted $S_2(1^1B_u)$ hereafter) corresponding to the ^1L_a zwitterionic state dominated by the HOMO→LUMO transition, with an out-of-phase mixing with the HOMO–1→LUMO+1 excitation. This state is calculated at 2.935 and 2.839 eV above S_0 for **1c** and **2c**, respectively. The second experimental absorption band of **2c** has a maximum at 470 nm (2.638 eV),[29] which corresponds to a 0.2 eV deviation from our XMCQDPT2 result, that is within the expected margin of errors for such methods. This state is usually targeted for triggering the photoisomerization as it leads to the formation of the CPD isomer[29,31] and CPD does not reabsorb in the visible range. Note that the respective covalent and zwitterionic nature of the ^1L_b and ^1L_a states is confirmed by analyzing their CASSCF wavefunctions using localized active orbitals on the atoms. In this way, the CASSCF wavefunction becomes equivalent to an extended valence-bond one, as it contains the covalent configurations (where every localized orbital is occupied by one electron) of a valence-bond representation and additional zwitterionic (or charge transfer) configurations (with some orbitals occupied by zero or two electrons). In the case of the $S_1(1^1A_u)$ ^1L_b state, the CASSCF wavefunction is dominated

by covalent configurations, while for the $S_2(1^1B_u)$ ^1L_a state, it is mainly described by zwitterionic configurations. It is thus not surprising to see that dynamic electron correlation is much more important in $S_2(1^1B_u)$ compared to $S_1(1^1A_u)$, as shown by the drastic reduction of the excitation energy for the zwitterionic state at post-CASSCF treatment (Tables 1 and 2).

The next excited state is the A_u^- state (denoted $S_3(2^1A_u)$ hereafter) described as a minus (out-of-phase) combination of the HOMO–1→LUMO and HOMO→LUMO+1 excitations. It is the *B_b* spectroscopic state located at 3.185 and 3.098 eV for **1c** and **2c**, respectively. This result is also within 0.2 eV of the experimental maximum of the third band at 377 nm (3.289 eV).[29]

The fourth brightest state is the B_u^+ state (denoted $S_4(2^1B_u)$ hereafter) and is dominated by the HOMO–1→LUMO+1 transition with an in-phase mixing with the HOMO→LUMO excitation. This spectroscopic *B_a* state peaks at 338 nm (3.668 eV),[29] in very good agreement with the vertical transitions computed at 3.708 and 3.657 eV for **1c** and **2c**, respectively.

The next two excited states, 1^1B_g and 2^1A_g, are dark states corresponding to symmetry-forbidden transitions and are located very close to each other at 3.9 and 4.0 eV, respectively. These two states are described by a mixture of singly- and doubly-excited configurations. Note that the 2^1A_g state has been identified as the state responsible for the existence of the photochemical funnel (conical intersection with the ground state 1^1A_g) allowing for the nonadiabatic DHP to CPD photoisomerization.[31] Regarding the absorption intensities, the computed oscillator strengths are consistent with the increasing absorbance going from the S_1 to the S_4 states.

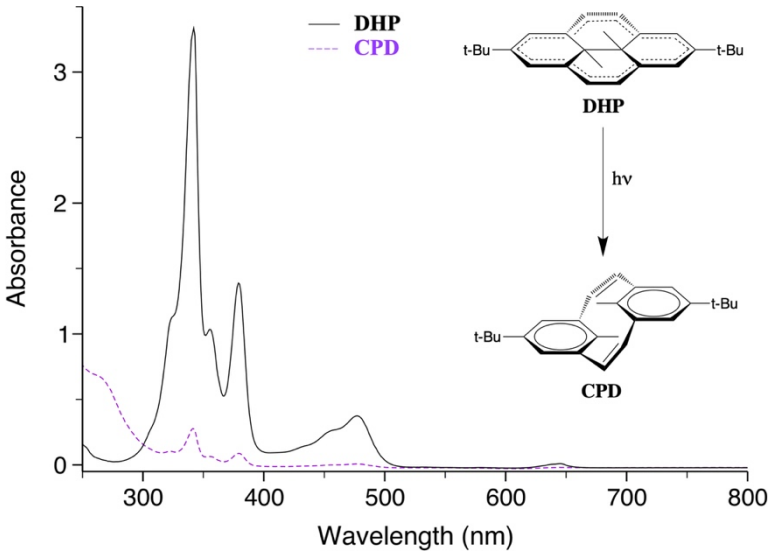

Figure 1. Spectra of a bis(t-butyl) DHP derivative[89] (full line) and of the corresponding CPD isomer (dashed line) in cyclohexane. Total irradiation time is 10 hours at $\lambda \geq 430$ nm. Note that traces of DHP are still present in the CPD spectrum, because of the thermal return (CPD→DHP).

Comparing the different wavefunction-based methods used here, Table 1 shows a good agreement between the MS-CASPT2 and XMCQDPT2 results for **1c**, with MS-CASPT2 outperforming CASPT2 for the transitions to the ^1B_u states for which substantial mixing is observed (the CASPT2 values are very close to the MS-CASPT2 ones except for 2^1B_u). However, Table 2 indicates that for **2c** MS-CASPT2 becomes unreliable for these states due to artificially too strong mixing. This mixing is more balanced in XMCQDPT2. NEVPT2 and QD-NEVPT2 underestimate the transitions to the ^1B_u states, in particular for the $S_2(1^1B_u)$ which is 0.6 and 0.9 eV below the MS-CASPT2 and XMCQDPT2 values for **2c**. This issue is encountered in electronic transitions involving zwitterionic states and requires increasing the active space with 3p orbitals to improve the results at the NEVPT2 level (Table S9 for an illustration on cyclopentadiene), a strategy not applicable here due to the system size. The single-reference ADC(2) method provides in general too high transition energies, while ADC(3) overcorrects ADC(2) giving too low transition energies. As reported in a recent benchmark study,[69] taking the average between the ADC(2) and ADC(3) transition energies yield rather accurate estimates: 1.921, 2.735, 3.373 and 3.913 eV

for the four lowest spectroscopic states of **2c**. Overall, the XMCQDPT2 seems to be the more robust method for computing the vertical transition energies of these simple DHPs.

The computationally efficient TD-DFT approach was also used in order to test various functionals. The purpose of these calculations is to choose a reliable functional in order to perform the simulation of the absorption spectra of DHPs and CPDs. Table 3 shows that the electronic structures of the excited states are well described, with the obvious exception of the 1^1B_g and 2^1A_g, for which the doubly-excited configurations are missing as TD-DFT is a single-excitation method. The order of the states is also reproduced and vertical transition energies are reasonably accurate for the four lowest bright states. While all functionals seem to overestimate the vertical transition energy to $S_1(1^1A_u)$, the best agreement is obtained for this state with CAM-B3LYP and ωB97XD. This is consistent with a recent TD-DFT study of **2c**.[40] The other transitions to the $S_2(1^1B_u)$, $S_3(2^1A_u)$ and $S_4(2^1B_u)$ states are all in good agreement with the experimental value for all the tested functionals.

Table 1. Vertical transition energies (eV), oscillator strengths and electronic configurations for DHP **1c**.

State	Configuration[a]	CI coeff.[b]	$\langle S_0 \vert \mu \vert S_n \rangle$ (f)[c]	CASSCF	CASPT2	MS-CASPT2	NEVPT2	QD-NEVPT2	XMC-QDPT2	ADC(2)/ ADC(3)
$S_0(1^1A_g)$	…$(H–1)^2(H)^2$	–0.78	–	–	–	–	–	–	–	–
$S_1(1^1A_u)$	…$(H–1)(H)^2(L)$	–0.56	0.09 (6.10^{-5})	1.848	2.006	2.059	2.078	2.077	1.978	2.296/ 1.678
	…$(H–1)^2(H)(L+1)$	–0.54								
$S_2(1^1B_u)$	…$(H–1)^2(H)(L)$	–0.74	1.27 (0.036)	4.711	2.837	2.777	2.109	2.097	2.935	2.980/ 2.760
	…$(H–1)(H)^2(L+1)$	+0.49								
$S_3(2^1A_u)$	…$(H–1)^2(H)(L+1)$	–0.60	6.06 (0.444)	5.442	3.372	3.372	2.945	2.950	3.185	3.550/ 3.458
	…$(H–1)(H)^2(L)$	+0.57								
$S_4(2^1B_u)$	…$(H–1)(H)^2(L+1)$	–0.66	9.05 (1.153)	6.083[d]	4.065	3.759	3.651	3.441	3.708	4.028/ 4.032
	…$(H–1)^2(H)(L)$	–0.45								
$S_5(1^1B_g)$	…$(H–2)(H–1)^2(H)^2(L)$	+0.37	0.0 (0.000)	3.978	4.092	4.089	4.192	4.177	3.881	4.519/ 3.210
	…$(H–1)^2(L)(L+1)$	–0.36								
$S_6(2^1A_g)$	…$(H–1)^2(L)^2$	+0.46	0.0 (0.000)	3.986	4.147	4.147	4.289	4.293	3.986	4.809/ n.c.[e]
	…$(H–3)(H–2)^2$ $(H–1)^2(H)^2(L)$	–0.37								

[a] CASSCF configurations obtained from state-averaged natural orbitals. H = HOMO, L = LUMO. [b] CASSCF configuration interaction coefficients obtained from state-averaged natural orbitals. Coefficients larger than 0.35 are given. [c] CASSCF transition dipole moments between ground and excited states in Debye and oscillator strengths f using XMCQDPT2 transition energies. [d] Corresponds to 4^1B_u at CASSCF level. [e] n.c.: not converged.

Table 2. Vertical transition energies (eV), oscillator strengths and electronic configurations for DHP **2c**.

State	Configuration[a]	CI coeff.[b]	$\langle S_0 \vert \mu \vert S_n \rangle$ (f)[c]	CASSCF	CASPT2	MS-CASPT2	NEVPT2	QD-NEVPT2	XMC-QDPT2	ADC(2)/ ADC(3)	Expt.[d]
$S_0(1^1A_g)$	…$(H–1)^2(H)^2$	+0.78	–	–	–	–	–	–	–	–	–
$S_1(1^1A_u)$	…$(H–1)(H)^2(L)$	+0.55	0.11 (9.10^{-5})	1.808	2.013	2.008	2.017	2.017	1.954	2.237/ 1.604	1.934
	…$(H–1)^2(H)(L+1)$	+0.55									
$S_2(1^1B_u)$	…$(H–1)^2(H)(L)$	+0.76	1.55 (0.026)	4.646	2.673	2.535	1.931	1.920	2.839	2.852/ 2.618	2.638
	…$(H–1)(H)^2(L+1)$	–0.46									
$S_3(2^1A_u)$	…$(H–1)^2(H)(L+1)$	–0.60	6.12 (0.439)	5.418	3.163	3.169	2.686	2.696	3.098	3.412/ 3.333	3.289
	…$(H–1)(H)^2(L)$	+0.59									
$S_4(2^1B_u)$	…$(H–1)(H)^2(L+1)$	–0.56	8.01 (0.889)	6.052[e]	4.426	3.093	4.342	3.382	3.657	3.919/ 3.907	3.668
	…$(H–1)^2(H)(L)$	–0.35									
$S_5(1^1B_g)$	…$(H–2)(H–1)^2(H)^2(L)$	–0.37	0.0 (0.000)	3.922	4.076	4.075	4.136	4.124	3.866	4.505/ 3.067	–
	…$(H–1)^2(L)(L+1)$	+0.37									
$S_6(2^1A_g)$	…$(H–1)^2(L)^2$	–0.49	0.0 (0.000)	3.916	4.082	4.083	4.201	4.210	3.931	4.714/ n.c.[e]	–
	…$(H–3)(H–2)^2$ $(H–1)^2(H)^2(L)$	+0.38									

[a] CASSCF configurations obtained from state-averaged natural orbitals. H = HOMO, L = LUMO. [b] CASSCF configuration interaction coefficients obtained from state-averaged natural orbitals. Coefficients larger than 0.35 are given. [c] CASSCF transition dipole moments between ground and excited states in Debye and oscillator strengths f using XMCQDPT2 transition energies. [d] Absorption maxima in cyclohexane (ε=2.0165).[29] [e] Corresponds to 4^1B_u at CASSCF level. [e] n.c.: not converged.

Table 3. Vertical transition energies (eV), oscillator strengths and electronic configurations using different functionals in DFT for DHP **2c**.

State	Configuration[a]	CI coeff.[b]	B3LYP[c]	B3PW91	CAM-B3LYP	PBE0	TPSSh	M06	M06-2X	ωB97XD
$S_0(1^1A_g)$	…$(H–1)^2(H)^2$	–	–	–	–	–	–	–	–	–
$S_1(1^1A_u)$	…$(H–1)(H)^2(L)$	+0.44	2.321 (0.002)	2.337	2.185 (0.002)	2.351	2.329	2.270	2.231	2.155
	…$(H–1)^2(H)(L+1)$	+0.55								
$S_2(1^1B_u)$	…$(H–1)^2(H)(L)$	+0.62	2.575 (0.018)	2.594	2.579 (0.020)	2.623	2.561	2.501	2.652	2.556
	…$(H–1)(H)^2(L+1)$	–0.34								
$S_3(2^1A_u)$	…$(H–1)^2(H)(L+1)$	–0.45	3.349 (0.264)	3.362	3.410 (0.284)	3.392	3.346	3.321	3.385	3.402
	…$(H–1)(H)^2(L)$	+0.55								
$S_4(2^1B_u)$	…$(H–1)(H)^2(L+1)$	+0.62	3.823 (0.791)	3.841	3.898 (0.856)	3.880	3.815	3.801	3.886	3.888
	…$(H–1)^2(H)(L)$	+0.34								
$S_5(1^1B_g)$	…$(H–1)^2(H)(L+2)$	+0.60	4.731 (0.000)	4.760	5.141 (0.000)	4.865	4.623	4.783	5.155	5.155
	…$(H–2)(H–1)^2(H)^2(L)$	–0.35								
$S_6(2^1A_g)$	…$(H–2)(H–1)^2(H)^2(L+1)$	+0.40	4.994 (0.000)	5.035	5.524 (0.000)	5.163	4.873	5.062	5.537	5.591
	…$(H–3)(H–2)^2(H–1)^2(H)^2(L)$	–0.38								

[a] TD-DFT configurations obtained at B3LYP level. H = HOMO, L = LUMO. [b] TD-DFT configuration interaction coefficients obtained at B3LYP level. Largest coefficients are given. [c] Oscillator strengths are given in parentheses.

Open-ring isomer. We now turn our attention to the CPD open-ring isomer. The two isomers **1o** and **2o** present excited states of similar nature and with comparable vertical excitation energies, as shown in Tables 4 and 5. Note that the HOMO and HOMO–1 of **1o** correlates with the HOMO–1 and HOMO of **2o**, respectively. The first two singlet excited states S_1 and S_2 are close in energy and depending on the level of theory the nature of these two states are interchanged. For **1o**, S_1 is the 1^1B_g state and S_2 is the 1^1B_u state in all cases. For **2o**, CASPT2 and MS-CASPT2 predict the S_1 state to be 1^1B_u in agreement with all the TD-DFT results reported in Table 6. Based on the present results, it is difficult to determine unambiguously the order of these two electronic states. Transition to the symmetry-allowed 1^1B_u state is expected to give rise to a weak absorption in the 3.6–3.7 eV region, in agreement with the weak absorption feature observed between 300–400 nm experimentally for CPDs.[30] The assignment of the third excited state is less problematic. All levels of theory agree with that state being the dark 2^1B_g state. It is located at 3.9–4.0 eV vertically above S_0. The fourth excited state is the 1^1A_u state located in the 4.1–4.3 eV energy range and the next one is the 2^1B_u lying only ca. 0.1 eV above it. These two states correspond to symmetry-allowed transitions and are expected to contribute to the intense absorption band arising below 300 nm. Then, a substantial energy gap is found to reach the next two excited states, 2^1A_u and 2^1A_g, as they were located at ca. 5.6–5.8 eV above S_0. Note that the dark 2^1A_g electronic structure is mainly built from doubly-excited configurations.

Comparing the ab initio methods, MS-CASPT2 and XMCQDPT2 are in reasonable agreement for the first five vertical transition energies of **1o** with differences not exceeding 0.26 eV. For the next two excited states, larger deviations of 0.5-0.6 eV are computed. For **2o**, while transition energies to S_1 and S_2 are within 0.2 eV between MS-CASPT2 and XMCQDPT2 values, the order of the states are reversed between these two methods. Good agreement is obtained for the next three states, but as for **1o**, larger deviations of 0.52 and 0.32 eV are computed for 2^1A_u and 2^1A_g, respectively. The statement regarding ADC(2) providing systematically too high transition energies and ADC(3) giving too low transition energies in **2c** does not seem to hold for the first five excited states of the open-ring isomer. In fact ADC(2) and ADC(3) give similar transition energies to these states in **2o**, and they are systematically higher than the

XMCQDPT2 values. Only for S_6 and S_7 one can notice again that ADC(2) overestimates and ADC(3) underestimates the transition energies. In the case of these simple CPDs, it is more difficult to conclude about the most accurate method, as the experimental spectrum does not show a simple structure as for DHPs and low-lying dark states play an important role.

Regarding the TD-DFT vertical transition energies, the results are comparable between B3LYP, B3PW91, PBE0, TPSSh and M06, while they are substantially different with CAM-B3LYP, M06-2X and ωB97XD. With these last three functionals, all the excited states investigated are blue shifted by a substantial amount of energy ranging from 0.2 eV up to 1 eV. If we consider that the first bright 1^1B_u is mainly responsible for the weak absorption feature predicted around 3.6 eV (~340 nm) by our accurate ab initio calculations and that the intense absorption in the 270-280 nm region is due to transitions to the 1^1A_u and 2^1B_u states (see discussion above), then CAM-B3LYP, M06-2X and ωB97XD clearly outperform B3LYP, B3PW91, PBE0, TPSSh and M06, as already reported in a previous study.[40]

Table 4. Vertical transition energies (eV), oscillator strengths and electronic configurations for CPD **1o**.

State	Configuration[a]	CI coeff.[b]	$\langle S_0 \vert \mu \vert S_n \rangle$ (*f*)[c]	CASSCF	CASPT2	MS-CASPT2	XMC-QDPT2	ADC(2)/ ADC(3)
$S_0(1^1A_g)$	…$(H–1)^2(H)^2$	–0.83	–	–	–	–	–	–
$S_1(1^1B_g)$	…$(H–1)^2(H)(L)$	–0.53	0.0 (0.000)	4.222	3.814	3.649	3.439	3.778/ 3.735
	…$(H–1)(H)^2(L+1)$	+0.47						
$S_2(1^1B_u)$	…$(H–1)(H)^2(L)$	+0.81	1.28 (0.024)	5.953	3.943	3.841	3.857	4.199/ 4.203
	…$(H–1)^2(H)(L+1)$	+0.23						
$S_3(2^1B_g)$	…$(H–1)(H)^2(L+1)$	–0.60	0.0 (0.000)	5.953	3.982	4.147	3.940	4.282/ 4.233
	…$(H–1)^2(H)(L)$	–0.60						
$S_4(1^1A_u)$	…$(H–2)(H–1)^2(H)^2(L)$	+0.42	0.36 (0.002)	4.558	4.445	4.440	4.177	4.650/ 4.439
	…$(H–1)(H)^2(L+2)$	–0.37						
$S_5(2^1B_u)$	…$(H–1)^2(H)(L+1)$	–0.74	4.58 (0.344)	6.907[d]	4.677	4.369	4.332[e]	4.890/ 5.092
	…$(H–1)(H)^2(L)$	+0.23						
$S_6(2^1A_u)$	…$(H–1)^2(L)(L+1)$	+0.29	0.52 (0.006)	6.359	5.968	5.973	5.381	5.720/ 5.274
	…$(H–1)(H)(L)^2$	+0.27						
$S_7(2^1A_g)$	…$(H–1)(H)(L)(L+1)$	+0.31	0.0 (0.000)	6.030	5.975	5.975	5.483	5.819/ 4.752
	…$(H–1)^2(L+1)^2$	+0.30						
	…$(H–2)^2(H)^2(L)^2$	+0.30						

[a] CASSCF configurations obtained from state-averaged natural orbitals. H = HOMO, L = LUMO. [b] CASSCF configuration interaction coefficients obtained from state-averaged natural orbitals. Largest coefficients are given. [c] CASSCF transition dipole moments between ground and excited states in Debye and oscillator strengths *f* using XMCQDPT2 transition energies. [d] Corresponds to 3^1B_u at CASSCF level. [e] Using (14e,14o) active space.

Table 5. Vertical transition energies (eV), oscillator strengths and electronic configurations for CPD **2o**.

State	Configuration[a]	CI coeff.[b]	$\langle S_0 \vert \mu \vert S_n \rangle$ (*f*)[c]	CASSCF	CASPT2	MS-CASPT2	XMC-QDPT2	ADC(2)/ ADC(3)	Expt.[d]
$S_0(1^1A_g)$	…$(H-1)^2(H)^2$	+0.83	–	–	–	–	–	–	–
$S_1(1^1B_g)$	…$(H-1)(H)^2(L)$	+0.50	0.0 (0.000)	4.173	3.780	3.702	3.482	3.752/ 3.745	n.a.[e]
	…$(H-1)^2(H)(L+1)$	–0.48							
$S_2(1^1B_u)$	…$(H-1)^2(H)(L)$	+0.83	1.48 (0.031)	5.812	3.639	3.487	3.661	3.908/ 3.948	n.a.[e]
	…$(H-1)(H)^2(L+1)$	+0.19							
$S_3(2^1B_g)$	…$(H-1)^2(H)(L+1)$	–0.60	0.0 (0.000)	6.045	3.903	3.984	3.920	4.177/ 4.161	n.a.[e]
	…$(H-1)(H)^2(L)$	–0.60							
$S_4(1^1A_u)$	…$(H-2)(H-1)^2(H)^2(L)$	+0.42	0.29 (0.001)	4.434	4.336	4.334	4.120	4.459/ 4.287	4.4–4.6
	…$(H-1)^2(H)(L+2)$	–0.38							
$S_5(2^1B_u)$	…$(H-1)(H)^2(L+1)$	+0.68	3.19 (0.170)	7.114[f]	5.122	4.427	4.411[g]	4.968/ 5.200	4.4–4.6
	…$(H-1)^2(H)(L)$	–0.13							
$S_6(2^1A_u)$	…$(H-1)(H)(L)^2$	+0.33	0.34 (0.003)	6.445	6.100	6.106	5.583	5.474/ 5.244	–
	…$(H-2)^2(H)^2(L)(L+1)$	+0.24							

$S_7(2^1A_g)$	…$(H–1)^2(L)^2$	–0.45	0.0 (0.000)	5.949	6.061	6.064	5.749	5.455/ 4.670	–
	…(H–1)(H)(L)(L+1)	–0.26							
	…(H–3)…(H)(L)(L+3)	–0.25							

[a] CASSCF configurations obtained from state-averaged natural orbitals. H = HOMO, L = LUMO. [b] CASSCF configuration interaction coefficients obtained from state-averaged natural orbitals. Largest coefficients are given. [c] CASSCF transition dipole moments between ground and excited states in Debye and oscillator strengths *f* using XMCQDPT2 transition energies. [d] Approximate absorption maxima in cyclohexane (ε=2.0165) (see Fig. 1). [e] Not available because the weak absorptions in the 300-400 nm region are hidden by the presence of unconverted DHP. [f] Corresponds to 3^1B_u at CASSCF level. [g] Using (14e,14o) active space.

Table 6. Vertical transition energies (eV), oscillator strengths and electronic configurations using different functionals in DFT for CPD **2o**.

State	Configuration[a]	CI coeff.[b]	B3LYP[c]	B3PW91	CAM-B3LYP	PBE0	TPSSh	M06	M06-2X	ωB97XD
$S_0(1^1A_g)$	…$(H–1)^2(H)^2$	–	–	–	–	–	–	–	–	–
$S_1(1^1B_g)$	…$(H–1)(H)^2(L)$	+0.69	3.308 (0.000)	3.320	3.772 (0.000)	3.415	3.196	3.372	3.773	3.793
	…$(H–1)^2(H)(L+1)$	+0.12								
$S_2(1^1B_u)$	…$(H–1)^2(H)(L)$	+0.70	3.185 (0.013)	3.188	3.630 (0.018)	3.271	3.084	3.208	3.650	3.656
$S_3(2^1B_g)$	…$(H–1)^2(H)(L+1)$	+0.69	3.509 (0.000)	3.521	3.944 (0.000)	3.608	3.427	3.543	3.945	3.970
	…$(H–1)(H)^2(L)$	–0.12								
$S_4(1^1A_u)$	…$(H–2)(H–1)^2(H)^2(L)$	+0.58	4.287 (0.005)	4.299	4.600 (0.002)	4.387	4.197	4.289	4.624	4.606
	…$(H–1)^2(H)(L+2)$	+0.37								
$S_5(2^1B_u)$	…$(H–1)(H)^2(L+1)$	+0.69	4.244 (0.196)	4.268	4.883 (0.358)	4.390	4.101	4.309	4.876	4.934
$S_6(2^1A_u)$	…$(H–1)^2(H)(L+2)$	+0.44	4.760 (0.026)	4.780	5.510 (0.175)	4.929	4.580	4.858	5.472	5.546
	…$(H–1)(H)^2(L+3)$	+0.43								
$S_7(2^1A_g)$	…$(H–3)…(H)^2(L)$	+0.59	4.553 (0.000)	4.562	5.197 (0.000)	4.717	4.361	4.689	5.250	5.209
	…$(H–1)^2(H)(L+3)$	+0.38								

[a] TD-DFT configurations obtained at B3LYP level. H = HOMO, L = LUMO. [b] TD-DFT configuration interaction coefficients obtained at B3LYP level. Largest coefficients are given. [c] Oscillator strengths are given in parentheses.

Absorption band structures. In this section, we present the results of the simulated photoabsorption spectra in comparison with the experimental ones. We first performed the FCHT simulations of **2c** (Fig. 2), **1c** (Fig. 3) and **1o** (Fig. 4). The TD-CAM-B3LYP vertical transition energies and oscillator strengths are given in Table S10 for comparison between the unsubstituted and the dimethyl-substituted systems. The comparison of the absorption spectra of **1c** and **2c** shows that they are very similar, with the spectrum of **1c** slightly blue-shifted, in agreement with the vertical transition energies (see Tables 1 and 2, and Table S10). These spectra look also in good agreement with the experimental spectra (see Fig. 1), displaying four bands of increasing intensity corresponding to the first four electronic transitions, consistent with their respective oscillator strengths.

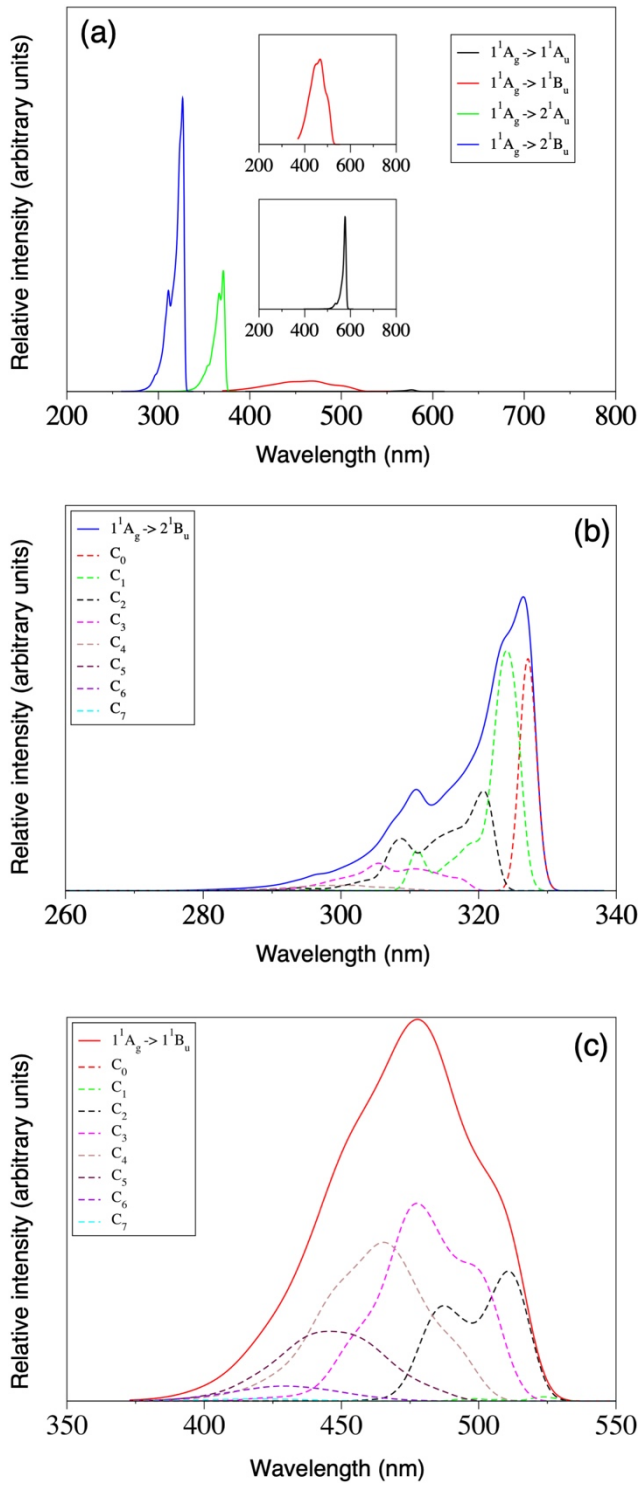

Figure 2. (a) FCHT absorption spectra of **2c** considering the electronic transitions from the ground to the lowest four excited states. Insets show an enlargement of the lowest two bands. (b) Decomposition of the highest intense band (2^1B_u state) in terms of classes C_n, partitioning the transitions based on the number n of simultaneously excited normal modes of the final electronic state. (c) Decomposition of the $S_0(1^1A_g) \rightarrow S_2(1^1B_u)$ band in terms of different classes C_n.

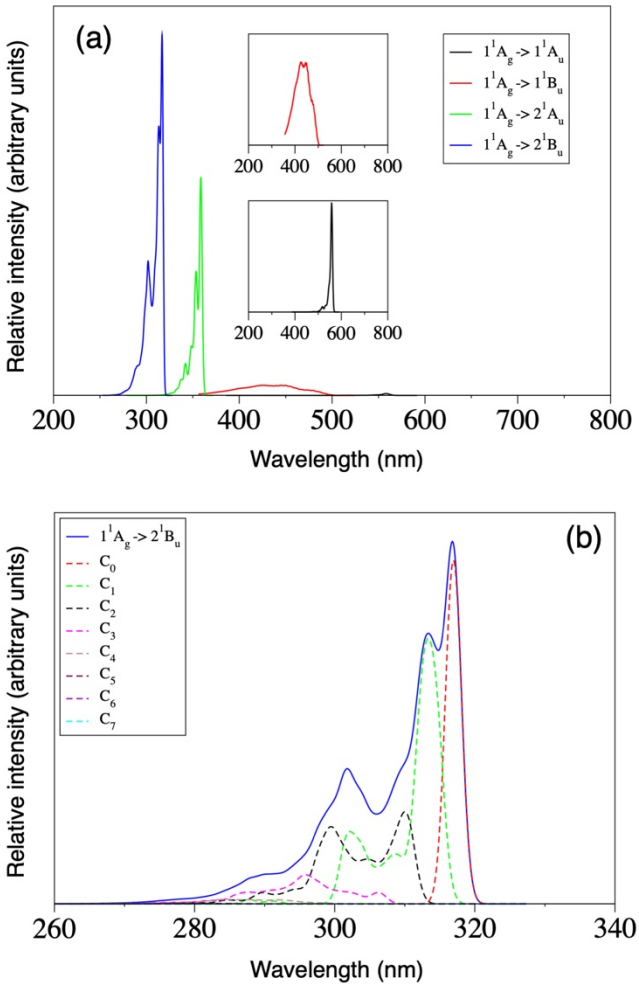

Figure 3. (a) FCHT absorption spectra of **1c** considering the electronic transitions from the ground to the lowest four excited states. Insets show an enlargement of the lowest two bands. (b) Decomposition of the highest intense band (2^1B_u state) in terms of classes C_n, partitioning the transitions based on the number n of simultaneously excited normal modes of the final electronic state.

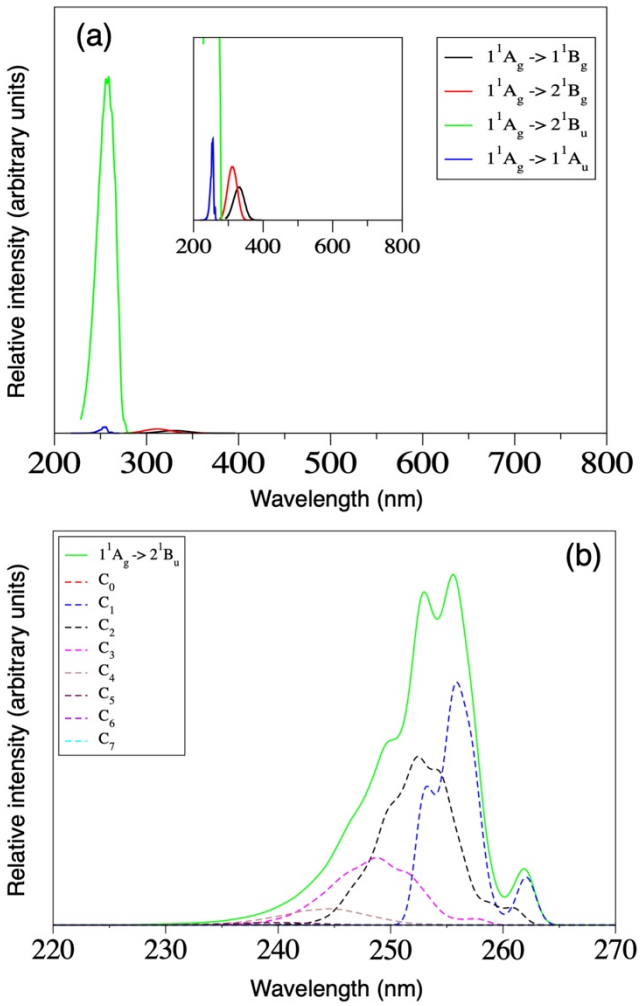

Figure 4. (a) FCHT absorption spectra of **1o** considering the electronic transitions from the ground to four excited states (ignoring the 1^1B_u state). Insets show an enlargement of the lowest three bands. (b) Decomposition of the highest intense band (2^1B_u state) in terms of classes C_n, partitioning the transitions based on the number n of simultaneously excited normal modes of the final electronic state.

The contributions in the **2c** overall spectrum of the 0-0 transition of $S_0(1^1A_g) \rightarrow S_1(1^1A_u)$, $S_0(1^1A_g) \rightarrow S_2(1^1B_u)$, $S_0(1^1A_g) \rightarrow S_3(2^1A_u)$ and $S_0(1^1A_g) \rightarrow S_4(2^1B_u)$ are ~48%, ~0.1%, ~26% and ~18%, respectively, while in **1c** these are ~65%, ~0.4%, ~43% and ~23%, respectively. It can be seen from these data that the intensity contribution of the 0-0 transition in the $S_0 \rightarrow S_2$ absorption band of **2c** and **1c** is quite low, which is in accordance with the large structural changes obtained in the energy minimum of the 1^1B_u state as shown Tables S5 and S6 (see change of dihedral angle ϕ values). These tables indicate that

$S_1(1^1A_u)$ has a similar geometry to S_0, while $S_2(1^1B_u)$ displays the largest structural changes among the excited states with respect to the ground-state structure. It is thus not surprising to find that the $S_0 \rightarrow S_1$ absorption is dominated by the 0-0 transition, while the $S_0 \rightarrow S_2$ absorption has the weakest contribution from the 0-0 transition.

The simulation of the FCHT absorption spectra of CPDs is more challenging theoretically. First, as noticed before, we could only simulate this spectrum for **1o** due to symmetry breaking in the excited states of **2o**. Second, there are two low-lying ^1B_g dark states which can only contribute to the simulated spectrum through the HT terms. These states could possibly contribute to the lowest absorption bands via vibronic couplings with the 1^1B_u state. Last but not least, the first bright 1^1B_u state has only one minimum on its own potential energy surface[31] (confirmed by our TD-DFT geometry optimizations) and its structure is more DHP-like than CPD-like (see Tables S5-S7). In other words, the 1^1B_u excited-state structure is so different from the ground-state CPD structure that the harmonic approximation does not hold. Hence, under these circumstances, we performed the FCHT simulation excluding the 1^1B_u state from our simulation. Figure 4 shows that the main absorption band at about 250 nm results from the $S_0(1^1A_g) \rightarrow S_5(2^1B_u)$ allowed transition, overlapping and hiding the very weak absorption band of the $S_4(1^1A_u)$ state. The two low-lying dark ^1B_g states contribute only weakly to the absorption features in the 300-400 nm range, due to intensity borrowing effects simulated through the HT couplings. The contributions of the 0-0 transitions in the overall intensity of the optically active $S_0(1^1A_g) \rightarrow S_4(1^1A_u)$ and $S_0(1^1A_g) \rightarrow S_5(2^1B_u)$ are ~1% and ~35%, respectively. This is in agreement with the larger structural changes computed in the 1^1A_u state than in the 2^1B_u state with respect to the ground state of **1o** (Table S7).

We now analyze, for some absorption bands, the contributions coming from the different class of excitations C_n, defined as the transitions to vibrational states involving simultaneous excitations of n normal modes of the final electronic state of the transition. Before focusing on the most intense absorption bands of **2c**, **1c** and **1o** in the spectral range considered in this study, we would like to discuss about the less intense $S_0(1^1A_g) \rightarrow S_2(1^1B_u)$ absorption band of **2c** (Figure 2c) following its importance as the targeted

state for photoisomerization. As discussed above and also mentioned in Ref. [31], the 1^1B_u state has only one minimum on its own potential energy surface. The corresponding structure is substantially different from the **2c** and **2o** minima. As a result of this, we find negligible contributions of the 0-0 transition and of transitions involving the excitation of a single mode (C_1). The absorption band of the present spectral transition is mainly obtained from multiple mode vibrational excitations (mainly from C_2, C_3, C_4 and C_5), with the largest contributions from C_3 and C_4. Hence, the absorption maximum of the present band is found around its center rather than at its onset, which is in good agreement with the experimental recording shown in Fig. 1.

The decomposition of the most intense bands in terms of intensity contributions from the different types of excitations C_n for **2c**, **1c** and **1o** is shown in Figs. 2b, 3b and 4b, respectively. The analysis of the figures Figs. 2b and 3b indicates that the contribution of C_n class, where $n \geq 3$, becomes flatter and flatter upon increasing *n*. This means that the contributions of simultaneous excitations of three or more vibrational modes have a small impact on the formation of overall shape of the most intense band of DHPs **2c** and **1c**. So, its shape results mainly from the contribution of the excitations of the 0-0 transition and of excitations of a maximum of two modes of the excited state. In the case of **1o**, the scenario is slightly different. The result of our simulation indicates that the spectrum is essentially dominated by C_1, C_2 and C_3. Noticeably, the contribution from the 0-0 transition is negligible in the formation of the most intense band of **1o**, unlike what is found for DHPs **1c** and **2c**. As a result, the maximum peak of the intense $S_0(1^1A_g) \rightarrow S_4(2^1B_u)$ absorption band of **1c** and **2c** is observed at the onset of this band, while in **1o** it is shifted towards the middle of band. Note that the agreement between the simulated and experimental band shapes of the S_3 and S_4 absorption of DHP are not so good, which could be due to vibronic couplings between these states.

The bottlenecks of the simulation of the CPD absorption spectra can be overcome by using the NE approach. The advantage of the in-built post-Condon approximation of the method is exploited to undertake the effect of optically dark states on the absorption spectrum. Also, the NE approach does not rely on the harmonic approximation, so the absorption related to the 1^1B_u state of the CPD molecule can

be simulated. We have applied the present methodology both for DHP **2c** and CPD **2o** and the corresponding results are shown in Figures 5 and 6.

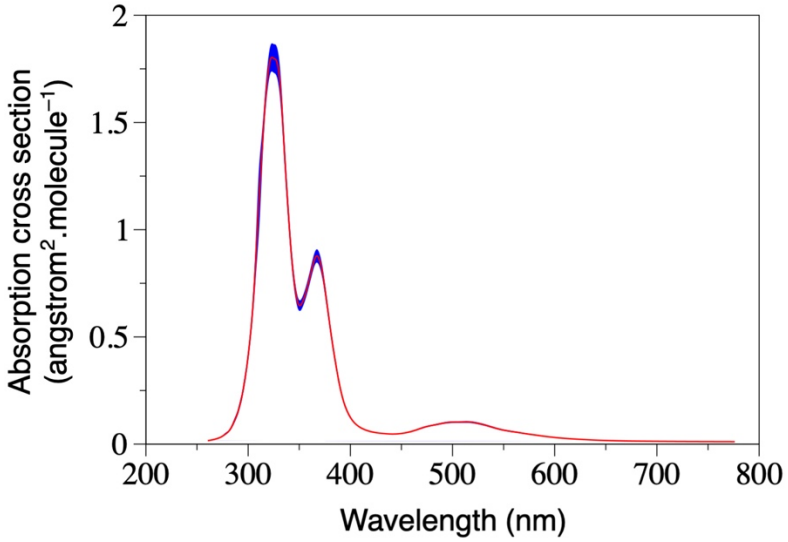

Figure 5. Simulated absorption spectrum of **2c** resulting from $S_0 \rightarrow S_1(1^1A_u)$, $S_0 \rightarrow S_2(1^1B_u)$, $S_0 \rightarrow S_3(2^1A_u)$ and $S_0 \rightarrow S_4(2^1B_u)$ electronic transitions using the NE approach. The blue area indicates the error in the absorption cross section due to the statistical sampling.

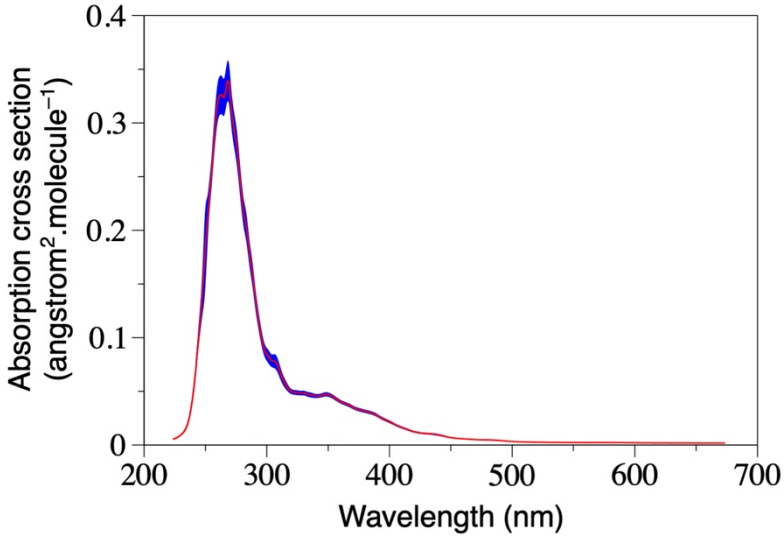

Figure 6. Simulated absorption spectrum of **2o** resulting from $S_0 \rightarrow S_1(1^1B_g)$, $S_0 \rightarrow S_2(1^1B_u)$, $S_0 \rightarrow S_3(2^1B_g)$, $S_0 \rightarrow S_4(1^1A_u)$ and $S_0 \rightarrow S_5(2^1B_u)$ electronic transitions using the NE approach. The blue area indicates the error in the absorption cross section due to the statistical sampling.

The comparison between the simulated absorption cross section of **2c** with available experimental spectra (see Fig. 1, but also Refs.[29,90]) indicates that overall the four absorption bands of DHP are nicely reproduced by the present NE approach. The band position of the lowest electronic transition, $S_0(1^1A_g)\rightarrow S_1(1^1A_u)$, is slightly blue shifted as compared to the experimental measurements, whereas for the next three electronic transitions, $S_0(1^1A_g)\rightarrow S_2(1^1B_u)$, $S_0(1^1A_g)\rightarrow S_3(2^1A_u)$ and $S_0(1^1A_g)\rightarrow S_4(2^1B_u)$, a better agreement is obtained. A similar observation can also be made for the FCHT spectrum of **2c** (Fig. 2a). These energy shifts are due to the underlying TD-DFT method that is used to compute the vertical transition energies (cf. Table 3) rather than to the method used to simulate the absorption spectrum. The overall intensities of the experimental bands of DHP are nicely reproduced by both simulation methods (cf. Fig. 1, Fig. 2a and Fig. 5).

The computed absorption cross section of CPD **2o** (Figure 6) compares satisfactorily with the experimental profile of the t-butyl substituted CPD shown in Fig. 1 in the energy range of ~400-240 nm. The NE simulation clearly outperforms the FCHT approach for wavelengths longer than 300 nm. Regarding the low-energy part of the spectrum (λ>300 nm), it is difficult to compare the experimental spectrum in Figure 1 and our simulation in Figure 6 because of incomplete photoconversion of the t-butyl substituted DHP even after hours of illumination, due to stationary state or to the thermal reverse reaction (CPD→DHP) that occurs during the photochemical reaction. This can be deduced from the very weak absorption remaining in the visible range around 480 nm (Fig. 1, purple line), which cannot be explained by the electronic transitions in CPD. The three humps observed in the absorption band of the t-butyl substituted CPD in the energy range ~400-340 nm are thus most likely the result of a small fraction of DHP that has not been converted into CPD at the photostationary state. However, Bohne et al. have shown that CPD compounds do display weak absorptions in the 300-400 nm region that are not due to unconverted DHPs.[30] Our simulation shows that these weak absorption features can be attributed to the post-Condon activity of the three lowest electronic transitions (one optically active and two optically dark)

of $1^1A_g \rightarrow 1^1B_u$, $1^1A_g \rightarrow 1^1B_g$, and $1^1A_g \rightarrow 2^1B_g$. The $S_0 \rightarrow S_4$ and $S_0 \rightarrow S_5$ transitions, resulting from the optically active 1^1A_u and 2^1B_u states, are responsible for the relatively steep rise of the absorption in the energy range ~300-240 nm. The two absorption bands of S_4 and S_5 clearly overlap (Figure S1) suggesting that non-adiabatic couplings (not taken into account in this study) between the 1^1A_u and 2^1B_u states are significant. Due to configuration mixing, we cannot assign the S_4 and S_5 absorption to either $1^1A_g \rightarrow 1^1A_u$ or $1^1A_g \rightarrow 2^1B_u$ transitions specifically.

4. CONCLUSIONS

In the present study, we report high-level vertical transition energy calculations of DHP and CPD isomers based on state-of-the-art ab initio calculations. The importance of having a balanced description of the covalent and ionic states proved crucial in these systems, requiring an accurate description of the differential dynamic electron correlation. The first four electronic transitions of DHP, $S_0(1^1A_g) \rightarrow S_1(1^1A_u)$, $S_0(1^1A_g) \rightarrow S_2(1^1B_u)$, $S_0(1^1A_g) \rightarrow S_3(2^1A_u)$ and $S_0(1^1A_g) \rightarrow S_4(2^1B_u)$, are symmetry-allowed and present increasing oscillator strengths. They are followed by two symmetry-forbidden transitions $S_0(1^1A_g) \rightarrow S_5(1^1B_g)$ and $S_0(1^1A_g) \rightarrow S_6(2^1A_g)$ involving states with substantial double-excitation character. In CPD, the scenario is very different, with three low-lying transitions involving two dark ^1B_g states and the weakly bright 1^1B_u state. These states are expected to be responsible for the weak absorption features between 300-400 nm. Higher energy symmetry-allowed transitions to the 1^1A_u and 2^1B_u states are good candidates for the increasing absorption observed at $\lambda < 300$ nm.

Comparison between reference ab initio methods and TD-DFT results is discussed in order to choose an appropriate functional to simulate the absorption spectra of these two isomers, including vibrational effects. These spectra were obtained using either the FCHT or the NE approaches. Overall, for both methods, the simulated spectra reproduce nicely the main spectral features of the DHP and CPD isomers, that is the main four absorption bands of increasing intensity of DHP and the absorption rise below 300 nm for CPD. Nevertheless, the NE simulation clearly outperforms the FCHT approach for the low-energy

part of the CPD spectrum between 300 and 400 nm, as the FCHT approach underestimates the absorption of the dark states and cannot reproduce the absorption band of the 1^1B_u state in contrast to the NE approach.

We have also shown that the dihydropyrene photochromic couple (**1c**/**1o**) presents very similar excited states and absorption features than its dimethyldihydropyrene counterpart (**2c**/**2o**), providing first evidences that dihydropyrene is a good model system for studying the DHP/CPD photoswitching behavior.

As a perspective for future work, inclusion of vibronic couplings need to be considered in order to describe more reliably the absorption spectra of DHPs and CPDs, in particular the band shapes. This could be done by studying non-adiabatic nuclear dynamics on the excited electronic states of DHP and CPD following a full quantum mechanical approach using time-dependent and time-independent methodologies.[9192,93,94] This task is however very challenging considering the large number of nuclear degrees of freedom in these systems.

Funding Sources

M.-C. Heitz, G. Royal and M. Boggio-Pasqua received funding from Agence Nationale de la Recherche through grant No. ANR-18-CE29-0012 (Photochromics project).

Supporting Information. Experimental section. Tables S1–S4 for CASSCF optimized geometries. Tables S5–S7 for geometrical distortions in the excited states of **1c**, **2c** and **1o**, respectively. Table S8 for substituent and solvent effects on DHP absorption spectrum. Table S9 for convergence of NEVPT2 transition energies to zwitterionic state depending on active space. Table S10 for vertical transition energies and oscillator strengths of **1c** and **2c** at TD-CAM-B3LYP level. Figure S1 for Oscillator strengths at NE sampled geometries of CPD **2o**

Acknowledgments. This work was granted access to the HPC resources of CALMIP supercomputing center under the allocation 2019-[12158]. The authors thank the LABEX NEXT for providing the funding of R. Sarkar's postdoctoral fellowship. We also thank David Sanchez for the installation of Q-CHEM on our local computing cluster.

References.

[1] Mitchell, R. H. The Metacyclophanediene-Dihydropyrene Photochromic π Switch. *Eur. J. Org. Chem.* **1999**, 2695–2703.

[2] Bouas-Laurent, H.; Dürr, H. Organic Photochromism. *Pure Appl. Chem.* **2001**, *73*, 639–665.

[3] Bakkar, A.; Lafolet, F.; Boggio-Pasqua, M.; Jouvenot, D.; Saint-Aman, E.; Cobo, S. Electrochemical Control of the Switching Process of Photochromic Dimethyldihydropyrene Derivatives. *Chem. Commun.* **2017**, *53*, 9360–9363.

[4] Cobo, S.; Lafolet, F.; Saint-Aman, E.; Philouze, C.; Bucher, C.; Silvi, S.; Credi, A.; Royal, G. Reactivity of a Pyridinium-Substituted Dimethyldihydropyrene Switch under Aerobic Conditions: Self-Sensitized Photo-Oxygenation and Thermal Release of Singlet Oxygen. *Chem. Commun.* **2015**, *51*, 13886–13889.

[5] Boggio-Pasqua, M.; López Vidal, M.; Garavelli, M. Theoretical Mechanistic Study of Self-Sensitized Photo-Oxygenation and Singlet Oxygen Thermal Release in a Dimethyldihydropyrene Derivative. *J. Photochem. Photobiol. A* **2017**, *333*, 156–164.

[6] Mitchell, R. H.; Ward, T. R.; Wang, Y.; Dibble, P. W. Pi-Switches: Synthesis of Three-Way Molecular Switches Based on the Dimethyldihydropyrene–Metacyclophanediene Valence Isomerization. *J. Am. Chem. Soc.* **1999**, *121*, 2601–2602.

[7] Mitchell, R. H.; Bohne, C.; Wang, Y.; Bandyopadhyay, S.; Wozniak, C. B. Multistate π Switches: Synthesis and Photochemistry of a Molecule Containing Three Switchable Annelated Dihydropyrene Units. *J. Org. Chem.* **2006**, *71*, 327–336.

[8] Muratsugu, S.; Kume, S.; Nishihara, H. Redox-Assisted Ring Closing Reaction of the Photogenerated Cyclophanediene Form of Bis(ferrocenyl)dimethyldihydropyrene with Interferrocene Electronic Communication Switching. *J. Am. Chem. Soc.* **2008**, *130*, 7204–7205.

[9] Muratsugu, S.; Kishida, M.; Sakamoto, R.; Nishihara, H. Comparative Study of Photochromic Ferrocene-Conjugated Dimethyldihydropyrene Derivatives. *Chem. Eur. J.* **2013**, *19*, 17314–17327.

[10] Vilà, N.; Royal, G.; Loiseau, F.; Deronzier, A. Photochromic and Redox Properties of Bisterpyridine Ruthenium Complexes Based on Dimethyldihydropyrene Units as Bridging Ligands. *Inorg. Chem.* **2011**, *50*, 10581–10591.

[11] Bakkar, A.; Cobo, S.; Lafolet, F.; Roldan, D.; Saint-Aman, E.; Royal, G. A Redox- and Photo-Responsive Quadri-State Switch Based on Dimethyldihydropyrene-Appended Cobalt Complexes. *J. Mater. C* **2016**, *4*, 1139–1143.

[12] Bakkar, A.; Cobo, S.; Lafolet, F.; Boggio-Pasqua, M.; Royal, G.; Saint-Aman, E. Self-Assembled Dimethyldihydropyrene-Pyridyl Substituted Ligands with Zinc(II) Meso-Tetraphenylporphyrin via Axial Coordination. *Dalton Trans.* **2016**, *45*, 16453–16462.

[13] Jacquet, M.; Lafolet, F.; Cobo, S.; Loiseau, F.; Bakkar, A.; Boggio-Pasqua, M.; Saint-Aman, E.; Royal, G. Efficient Photoswitch System Combining a Dimethyldihydropyrene Pyridinium Core and Ruthenium(II) Bis-Terpyridine Entities. *Inorg. Chem.* **2017**, *56*, 4357–4368.

[14] Roldan, D.; Kaliginedi, V.; Cobo, S.; Kolivoska, V.; Bucher, C.; Hong, W.; Royal, G.; Wandlowski, T. Charge Transport in Photoswitchable Dimethyldihydropyrene-Type Single-Molecule Junctions. *J. Am. Chem. Soc.* **2013**, *135*, 5974–5977.

[15] Bakkar, A.; Lafolet, F.; Roldan, D.; Puyoo, E.; Jouvenot, D.; Royal, G.; Saint-Aman, E.; Cobo, S. Bidirectional Light-Induced Conductance Switching in Molecular Wires Containing a Dimethyldihydropyrene Unit. *Nanoscale* **2018**, *10*, 5436–5441.

[16] Tsuji, Y.; Hoffmann, R. Frontier Orbital Control of Molecular Conductance and it Switching. *Angew. Chem. Int. Ed.* **2014**, *126*, 4177–4181.

[17] Zhang, G. P.; Mu, Y. Q.; Zhao, J. M.; Huang, H.; Hu, G. C.; Li, Z. L.; Wang, C. K. Optimizing the Conductance Switching Performance in Photoswitchable Dimethyldihydropyrene/Cyclophanediene Single-Molecule Junctions. *Physica E* **2019**, *109*, 1–5.

[18] Straight, S. D.; Andréasson, J.; Kodis, G.; Bandyopadhyay, S.; Mitchell, R. H.; Moore, T. A.; Moore, A. L.; Gust, D. Molecular AND and INHIBIT Gates Based on Control of Porphyrin Fluorescence by Photochromes. *J. Am. Chem. Soc.* **2005**, *127*, 9403–9409.

[19] Klaue, K.; Garmshausen, Y.; Hecht, S. Taking Photochromism beyond Visible: Direct One-Photon NIR Photoswitches Operating in the Biological Window. *Angew. Chem. Int. Ed.* **2018**, *57*, 1414–1417.

[20] Mitchell, R. H.; Brkic, Z.; Sauro, V. A.; Berg, D. J. A Photochromic, Electrochromic, Thermochromic Ru Complexed Benzannulene: an Organic Example of the Dimethyldihydropyrene–Metacyclophanediene Valence Isomerization. *J. Am. Chem. Soc.* **2003**, *125*, 7581–7585.

[21] Mitchell, R. H.; Ward, T. R.; Chen, Y.; Wang, Y.; Weerawarna, S. A.; Dibble, P. W.; Marsella, M. J.; Almutairi, A.; Wang, Z.-Q. Synthesis and Photochromic Properties of Molecules Containing [*e*]-Annelated Dihydropyrenes. Two and Three Way π-Switches Based on the Dimethyldihydropyrene–Metacyclophanediene Valence Isomerization. *J. Am. Chem. Soc.* **2003**, *125*, 7581–7585.

[22] Williams, R. V.; Edwards, W. D.; Mitchell, R. H.; Robinson, S. G. A DFT Study of the Thermal, Orbital Symmetry Forbidden, Cyclophanediene to Dihydropyrene Electrocyclic Reaction. Predictions to Improve the Dimethyldihydropyrene Photoswitches. *J. Am. Chem. Soc.* **2005**, *127*, 16207–16214.

[23] Mitchell, R. H.; Bohne, C.; Robinson, S. G.; Yang, Y. The Effect of Addition of Fluorescent Moieties to Dihydropyrenes: Enhancing Photochromicity and Fluorescence Monitoring. *J. Org. Chem.* **2007**, *72*, 7939–7946.

[24] Ayub, K.; Li, R.; Bohne, C.; Williams, R. V.; Mitchell, R. H. Calculation Driven Synthesis of an Excellent Dihydropyrene Negative Photochrome and its Photochemical Properties. *J. Am. Chem. Soc.* **2011**, *133*, 4040–4045.

[25] Ayub, K.; Mitchell, R. H. Syntheses of Dihydropyrene–Cyclophanediene Negative Photochromes Containing Internal Alkenyl and Alkynyl Groups and Comparison of Their Photochemical and Thermochemical Properties. *J. Org. Chem.* **2014**, *79*, 664–678.

[26] Roldan, D.; Cobo, S.; Lafolet, F.; Vilà, N.; Bochot, C.; Bucher, E.; Saint-Aman, E.; Boggio-Pasqua, M.; Garavelli, M.; Royal, G. A Multi-Addressable Switch Based on the Dimethyldihydropyrene Photochrome with Remarkable Proton-Triggered Photo-opening Efficiency. *Chem.-Eur. J.* **2015**, *21*, 455–467.

[27] Boggio-Pasqua, M.; Garavelli, M. Rationalization and Design of Enhanced Photoinduced Cycloreversion in Photochromic Dimethyldihydropyrenes by Theoretical Calculations. *J. Phys. Chem. A* **2015**, *119*, 6024–6032.

[28] Murphy, R. S.; Chen, Y; Ward, T. R.; Mitchell, R. H.; Bohne, C. Photophysical Studies on the Photochromism of trans-10b,10c-Dimethyldihydropyrene. *Chem. Commun.* **1999**, 2097–2098.

[29] Sheepwash, M. A. L.; Mitchell, R. H.; Bohne, C. Mechanistic Insights into the Photochromism of *trans*-10b,10c-Dimethyl-10b-10c-dihydropyrene Derivatives. *J. Am. Chem. Soc.* **2002**, *124*, 4693–4700.

[30] Sheepwash, M. A. L.; Ward, T. R.; Wang, Y.; Bandyopadhyay, S.; Mitchell, R. H.; Bohne, C. Mechanistic Studies on the Photochromism of [e]-Annelated Dimethyldihydropyrenes. *Photochem. Photobiol. Sci.* **2003**, *2*, 104–112.

[31] Boggio-Pasqua, M.; Bearpark, M. J.; Robb, M. A. Toward a Mechanistic Understanding of the Photochromism of Dimethyldihydropyrenes. *J. Org. Chem.* **2007**, *72*, 4497–4503.

[32] Bohne, C.; Mitchell, R. H. Characterization of the Photochromism of Dihydropyrenes with Photophysical Techniques. *J. Photochem. Photobiol. C-Photochem. Rev.* **2011**, *12*, 126–137.

[33] Ayub, K.; Zhang, R.; Robinson, S. G.; Twamley, B.; Williams, R. V.; Mitchell, R. H. Suppressing the Thermal Metacyclophanediene to Dihydropyrene Isomerization: Synthesis and Rearrangement of 8,16-Dicyano[2.2]metacyclophane-1,9-diene and Evidence Supporting the Proposed Biradicaloid Mechanism. *J. Org. Chem.* **2008**, *73*, 451–456.

[34] Boggio-Pasqua, M.; Bearpark, M. J.; Hunt, P. A.; Robb, M. A. Dihydroazulene/Vinylheptafulvene Photochromism: A Model for One-Way Photochemistry via a Conical Intersection. *J. Am. Chem. Soc*. **2002**, *124*, 1456−1470.

[35] Boggio-Pasqua, M.; Ravaglia, M.; Bearpark, M. J.; Garavelli, M.; Robb, M. A. Can Diarylethene Photochromism Be Explained by a Reaction Path Alone? A CASSCF Study with Model MMVB Dynamics. *J. Phys. Chem. A* **2003**, *107*, 11139–11152.

[36] Boggio-Pasqua, M.; Bearpark, M. J.; Ogliaro, F.; Robb, M. A. Photochemical Reactivity of 2-Vinylbiphenyl and 2-Vinyl-1,3-terphenyl: The Balance between Nonadiabatic and Adiabatic Photocyclization. *J. Am. Chem. Soc.* **2006**, *128*, 10533–10540.

[37] Tomasello, G.; Bearpark, M. J.; Robb, M. A.; Orlandi, G.; Garavelli, M. Significance of a Zwitterionic State in Fulgide Photochromism: Implications for the Design of Mimics, *Angew. Chem. Int. Ed.* **2010**, *49*, 2913–2916.

[38] Iravani, M.; Omidyan, R. Excited-State Intramolecular Proton Transfer and Photoswitching in Hydroxyphenyl-Imidazopyridine Derivatives: A Theoretical Study. *J. Chem. Phys.* **2016**, *145*, 184303.

[39] Iravani, M.; Omidyan, R. Photochromism of 2-(2-Hydroxyphenyl) Benzothiazole (HBT) and Its Derivatives: A Theoretical Study. *J. Phys. Chem. A* **2018**, *122*, 3182–3189.

[40] Saima, B.; Khan, N.; Al-Faiyz, Y. S. S.; Ludwig, R.; Rehman, W.; Habib-ur-Rehman, M.; Sheikh, N. S.; Ayub, K. Photo-tunable Linear and Nonlinear Optical Response of Cyclophanediene-Dihydropyrene Photoswitches. *J. Mol. Graph. Model.* **2019**, *88*, 261–272.

[41] Robb, M. A. Theoretical Chemistry for Electronic Excited States; Theoretical and Computational Chemistry Series; The Royal Society of Chemistry, 2018. (DOI: 10.1039/9781788013642).

[42] Boggio-Pasqua, M.; Bearpark, M. J.; Klene, M.; Robb, M. A. A Computational Strategy for Geometry Optimization of Ionic and Covalent Excited States, Applied to Butadiene and Hexatriene. *J. Chem. Phys.* **2004**, *120*, 7849–7860.

[43] Dong, S. S.; Gagliardi, L.; Truhlar, D. G. Nature of the 1^1B_u and 2^1A_g Excited States of Butadiene and the Goldilocks Principle of Basis Set Diffuseness. *J. Chem. Theory Comput.* **2019**, *15*, 4591–4601.

[44] Tran, T.; Segarra-Martí, J.; Bearpark, M. J.; Robb, M. A. Molecular Vertical Excitation Energies Studied with First-Order RASSCF (RAS[1,1]): Balancing Covalent and Ionic Excited States. *J. Phys. Chem. A* **2019**, *123*, 5223–5230.

[45] Roca-Sanjuán, D.; Aquilante, F.; Lindh, R. Multiconfiguration Second-Order Perturbation Theory Approach to Strong Electron Correlation in Chemistry and Photochemistry. *WIREs Comput. Sci.* **2012**, *2*, 585–603.

[46] González, L.; Escudero, D.; Serrano-Andrés, L. Progress and Challenges in the Calculation of Electronic Excited States. *ChemPhysChem* **2012**, *13*, 28–51.

[47] Lischka, H.; Nachtigallová, D.; Aquino, A. J. A.; Szalay, P. G.; Plasser, F.; Machado, F. B. C.; Barbatti, M. Multireference Approaches for Excited States of Molecules. *Chem. Rev.* **2018**, *118*, 7293–7361.

[48] Veryazov, V.; Malmqvist, P. Å.; Roos, B. O. How to Select Active Space for Multiconfigurational Quantum Chemistry? *Int. J. Quantum Chem.* **2011**, *111*, 3329–3338.

[49] Casida, M. E.; Huix-Rotllant, M. Progress in Time-Dependent Density-Functional Theory. *Annu. Rev. Phys. Chem.* **2012**, *63*, 287–323.

[50] Mitchell, R. H.; Boekelheide, V. Transformation of Sulfide Linkages to Carbon-Carbon Double Bond. Syntheses of cis- and trans-15,16-Dimethyldihydropyrene and trans-15,16-Dihydropyrene. *J. Am. Chem. Soc.* **1974**, *96*, 1547–1557.

[51] Andersson, K.; Malmqvist, P. Å.; Roos, B. O. Second-Order Perturbation Theory with a CASSCF Reference Function. *J. Chem. Phys.* **1990**, *94*, 5483–5488.

[52] Finley, J.; Malmqvist, P.-Å.; Roos, B. O.; Serrano-Andrés, L. The Multi-State CASPT2 Method. *Chem. Phys. Lett.* **1998**, *288*, 299–306.

[53] Angeli, C.; Cimiraglia, R.; Evangelisti, S.; Leininger, T.; Malrieu, J.-P. Introduction of *n*-Electron Valence States for Multireference Perturbation Theory. *J. Chem. Phys.* **2001**, *114*, 10252–10264.

[54] Angeli, C.; Borini, S.; Cavallini, A.; Cestari, M.; Cimiraglia, R.; Ferrighi, A.; Sparta, M. Developments in the *n*-Electron Valence State Perturbation Theory. *Int. J. Quantum Chem.* **2006**, *106*, 686–691.

[55] Granovsky, A. A. Extended Multi-Configuration Quasi-Degenerate Perturbation Theory: The New Approach to Multi-State Multi-Reference Perturbation Theory. *J. Chem. Phys.* **2011**, *134*, 214113.

[56] Aquilante, F.; Autschbach, J.; Carlson, R. K.; Chibotaru, L. F.; Delcey, M. G.; De Vico, L.; Galván, I. F.; Ferré, N.; Frutos, L. M.; Gagliardi, L.; et al. MOLCAS 8: New Capabilities for Multiconfigurational Quantum Chemical Calculations across the Periodic Table. *J. Comput. Chem.* **2016**, *37*, 506–541.

[57] Ghigo, G.; Roos, B. O.; Malmqvist, P.-Å. A Modified Definition of the Zeroth-Order Hamiltonian in Multiconfigurational Perturbation Theory (CASPT2). *Chem. Phys. Lett.* **2004**, *396*, 142–149.

[58] Zobel, J. P.; Nogueira, J. J.; González, L. The IPEA Dilemma in CASPT2. *Chem. Sci.* **2017**, *8*, 1482–1499.

[59] Forsberg, N.; Malmqvist, P.-Å. Multiconfiguration Perturbation Theory with Imaginary Level Shift. *Chem. Phys. Lett.* **1997**, *274*, 196–204.

[60] Aquilante, F.; Malmqvist, P. Å.; Pedersen, T. B.; Ghosh, A.; Roos, B. O. Cholesky Decomposition-Based Multiconfiguration Second-Order Perturbation Theory (CD-CASPT2): Application to the Spin-State Energetics of Co^{III}(diiminato)(NPh). *J. Chem. Theory Comput.* **2008**, *4*, 694–702.

[61] Izsák, R.; Neese, F. An Overlap Fitted Chain of Spheres Exchange Method. *J. Chem. Phys.* **2011**, *135*, 144105.

[62] Neese, F. The ORCA Program System. *WIREs Comput. Mol. Sci.* **2012**, *2*, 73–78.

[63] Granovsky, A. A. Firefly version 8.2.0, www http://classic.chem.msu.su/gran/firefly/index.html.

[64] Dunning, T. H. Gaussian Basis Sets for Use in Correlated Molecular Calculations. I. The Atoms Boron through Neon and Hydrogen. *J. Chem. Phys.* **1989**, *90*, 1007–1023.

[65] Werner, H.-J.; Knowles, P. J.; Knizia, G.; Manby, F. R.; Schütz, M. Molpro: A General-Purpose Quantum Chemistry Program Package. *WIREs Comput. Mol. Sci.* **2012**, *2*, 242–253.

[66] Schirmer, J. Beyond the Random-Phase Approximation: A New Approximation Scheme for the Polarization Propagator. *Phys. Rev. A* **1982**, *26*, 2395–2416.

[67] Harbach, P. H. P.; Wormit, M.; Dreuw, A. The Third-Order Algebraic Diagrammatic Construction Method (ADC(3)) for the Polarization Propagator for Closed-Shell Molecules: Efficient Implementation and Benchmarking. *J. Chem. Phys.* **2014**, *141*, 064113.

[68] Christiansen, O.; Koch, H.; Jørgensen, P. Response Functions in the CC3 Iterative Triplet Excitation Model. *J. Chem. Phys.* **1995**, *103*, 7429–7441.

[69] Koch, H.; Christiansen, O.; Jørgensen, P.; Sanchez de Merás, A. M.; Helgaker T. The CC3 Model: An Iterative Coupled Cluster Approach Including Connected Triples. *J. Chem. Phys.* **1997**, *106*, 1808–1818.

[70] Loos, P.-F.; Scemama, A.; Blondel, A.; Garniron, Y.; Caffarel, M.; Jacquemin, D. A Mountaineering Strategy to Excited States: Highly Accurate Reference Energies and Benchmarks. *J. Chem. Theory Comput.* **2018**, *14*, 4360–4379.

[71] Loos, P.-F.; Boggio-Pasqua, M.; Scemama, A.; Caffarel, M.; Jacquemin, D. Reference Energies for Double Excitations. *J. Chem. Theory Comput.* **2019**, *15*, 1939–1956.

[72] Shao, Y. S.; Gan, Z.; Epifanovsky, E.; Gilbert, A. T. B.; Wormit, M.; Kussmann, J.; Lange, A. W.; Behn, A.; Deng, J.; Feng, X. et al. Advances in Molecular Quantum Chemistry Contained in the Q-Chem 4 Program Package. *Mol. Phys.* **2015**, *113*, 184–215.

[73] Frisch, M. J.; Trucks, G. W.; Schlegel, H. B.; Scuseria, G. E.; Robb, M. A.; Cheeseman, J. R.; Scalmani, G.; Barone, V.; Petersson, G. A.; Nakatsuji, H.; et al. *Gaussian 09, revision D.01*, Gaussian, Inc., Wallingford CT, 2009.

[74] Becke, A. D. Density-Functional Thermochemistry. III. The Role of Exact Exchange. *J. Chem. Phys.* **1993**, *98* 5648–5652.

[75] Perdew, J. P.; Wang, Y. Accurate and Simple Analytic Representation of the Electron-Gas Correlation Energy. *Phys. Rev. B* **1992**, *45*, 13244–13249.

[76] Adamo, C.; Barone, V. Toward Reliable Density Functional Methods without Adjustable Parameters: The PBE0 Model. *J. Chem. Phys.* **1999**, *110*, 6158–6170.

[77] Tao, J.; Perdew, J. P.; Staroverov, V. N.; Scuseria, G. E. Climbing the Density Functional Ladder: Nonempirical Meta–Generalized Gradient Approximation Designed for Molecules and Solids. *Phys. Rev. Lett.* **2003**, *91*, 146401.

[78] Zhao, Y.; Truhlar, D. G. The M06 Suite of Density Functionals for Main Group Thermochemistry, Thermochemical Kinetics, Noncovalent Interactions, Excited States, and Transition Elements: Two New Functionals and Systematic Testing of Four M06-Class Functionals and 12 Other Functionals. *Theor. Chem. Acc.* **2008**, *120*, 215–241.

[79] Yanai, T.; Tew, D. P.; Handy, N. C. A New Hybrid Exchange–Correlation Functional using the Coulomb-Attenuating Method (CAM-B3LYP). *Chem. Phys. Lett.* **2004**, *393*, 51–57.

[80] Chai, J.-D.; Head-Gordon, M. Long-Range Corrected Hybrid Density Functionals with Damped Atom–Atom Dispersion Corrections. *Phys. Chem. Chem. Phys.* **2008**, *10*, 6615–6620.

[81] Barone, V.; Bloino, J.; Biczysko, M.; Santoro, F. Fully Integrated Approach to Compute Vibrationally Resolved Optical Spectra: From Small Molecules to Macrosystems. *J. Chem. Theory Comput.* **2009**, *5*, 540−554.

[82] Duschinsky, F. Zur Deutung der Elekronenspektren Mehratomiger Molekule I. Uber das Franck-Condon-Prinzip. *Acta Physicochimica URSS* **1937,** *7*, 551–556.

[83] Crespo-Otero, R.; Barbatti, M. Spectrum Simulation and Decomposition with Nuclear Ensemble: Formal Derivation and Application to Benzene, Furan and 2-Phenylfuran. *Theor. Chem. Acc.* **2012,** 131, 1237.

[84] Barbatti, M.; Sen, K. Effects of Different Initial Condition Samplings on Photodynamics and Spectrum of Pyrrole. *Int. J. Quantum Chem.* **2016,** *116*, 762–771.

[85] Barbatti, M.; Granucci, G.; Persico, M.; Ruckenbauer, M.; Vazdar, M.; Eckert-Maksić, M.; Lischka, H. The On-the-Fly Surface-Hopping Program System Newton-X: Application to Ab Initio Simulation of

the Nonadiabatic Photodynamics of Benchmark Systems *J. Photochem. Photobiol. A-Chem.* **2007,** *190*, 228–240.

[86] Barbatti, M.; Granucci, G.; Ruckenbauer, M.; Plasser, F.; Pittner, J.; Persico, M.; Lischka, H. NEWTON-X: a Package for Newtonian Dynamics Close to the Crossing Seam, version 1.4, www.newtonx.org (2013).

[87] Barbatti, M.; Ruckenbauer, M.; Plasser, F.; Pittner, J.; Granucci, G.; Persico, M.; Lischka, H. Newton-X: A Surface-Hopping Program for Nonadiabatic Molecular Dynamics. *WIREs Comput. Mol. Sci.* **2014**, *4*, 26–33.

[88] Platt, J. R. Classification of Spectra of Cata-Condensed Hydrocarbons. *J. Chem. Phys.* **1949**, *17*, 484–495.

[89] Note that the bis(t-butyl) DHP derivative displays a very similar photoabsorption spectrum as compound **2c**, according to Ref. [29]. See also Table S8.

[90] Boekelheide V.; Phillips. J. B. Aromatic Molecules Bearing Substituents within the Cavity of the π-Electron Cloud. Synthesis of *trans*-15,16-Dimethyldihydropyrene. *J. Am. Chem. Soc.* **1967**, *89*, 1695–1704.

[91] Köppel, H.; Domcke, W.; Cederbaum, L. S. Multimode Molecular Dynamics beyond the Born-Oppenheimer Approximation. *Adv. Chem. Phys.* **1984**, *57*, 59–246.

[92] Beck, M. H.; Jäckle, A.; Worth, G. A.; Meyer, H.-D. The Multiconfiguration Time-Dependent Hartree (MCTDH) Method: a Highly Efficient Algorithm for Propagating Wavepackets. *Phys. Rep.* **2000**, *324*, 1–105.

[93] Worth, G. A.; Cederbaum, L. S. Beyond Born-Oppenheimer: Molecular Dynamics through a Conical Intersection. *Annu. Rev. Phys. Chem.* **2004**, *55*, 127–158.

[94] Worth, G. A.; Meyer, H.-D.; Köppel, H.; Cederbaum, L. S.; Burghardt, I. Using the MCTDH Wavepacket Propagation Method to Describe Multimode Non-Adiabatic Dynamics. *Int. Rev. Phys Chem.* **2008**, *27*, 569–606.

TOC Graphic.

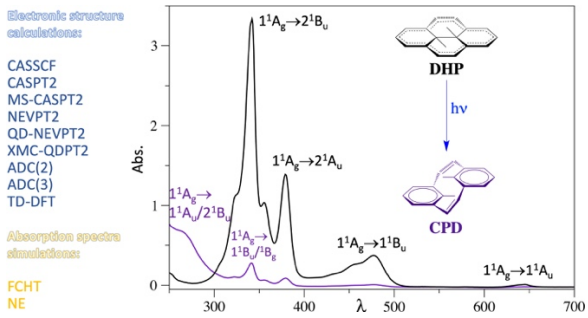
Electronic structure calculations:
CASSCF
CASPT2
MS-CASPT2
NEVPT2
QD-NEVPT2
XMC-QDPT2
ADC(2)
ADC(3)
TD-DFT
Absorption spectra simulations:
FCHT
NE
Abs.
λ
300
400
500
600
700
0
1
2
3
$1^1A_g \rightarrow 2^1B_u$
$1^1A_g \rightarrow 2^1A_u$
$1^1A_g \rightarrow 1^1B_u$
$1^1A_g \rightarrow 1^1A_u$
$1^1A_g \rightarrow 1^1A_u/2^1B_u$
$1^1A_g \rightarrow 1^1B_u/1^1B_g$
DHP
hv
CPD